

Topological Structure is Predictive of Deep Neural Network Success in Learning

Christopher Griffin,¹ Trevor Karn,² and Benjamin Apple³

¹*Applied Research Laboratory, The Pennsylvania State University, University Park, PA 16802*

²*School of Mathematics, University of Minnesota, Minneapolis, MN 55455*

³*Naval Surface Warfare Center Carderock MD, 20817*

(Dated: January 25, 2023 - Preprint)

Machine learning has become a fundamental tool in modern science, yet its limitations are still not fully understood. Using a simple children's game, we show that the topological structure of the underlying training data can have a dramatic effect on the ability of a deep neural network (DNN) classifier to learn to classify data. We then take insights obtained from this toy model and apply them to two physical data sets (one from particle physics and one from acoustics), which are known to be amenable to classification by DNN's. We show that the simplicity in their topological structure explains the majority of the DNN's ability to operate on these data sets by showing that fully interpretable topological classifiers are able to perform nearly as well as their DNN counterparts.

I. INTRODUCTION

The use of deep learning methods in particular and artificial intelligence in general has become ubiquitous in science (see [1–20] for a small example set). Recent work has shown that DNN's are able to generalize fundamental physical principles like symmetry [11]. Yet we still lack a fundamental understanding of when these techniques can be successfully applied [21–24] and in some sense the *no free lunch* theorems [21, 22] imply it is impossible to know *a priori* whether a data set is amenable to an off-the-shelf deep learning approach. Despite the fact that deep learning methods seem to frequently work, we may simply be observing a positive result bias [25]. In this paper, we use a variation on topological data analysis to understand when deep neural network (DNN) classifiers work well and when they work poorly in a simple children's game, *Math Dice Jr.* We then show the utility of the approach by using topological information to explain why two physics-based classification problems are easily solved by deep learning techniques (see Fig. 1). In particular, we show that the geometric structure of the data sets in question is topologically

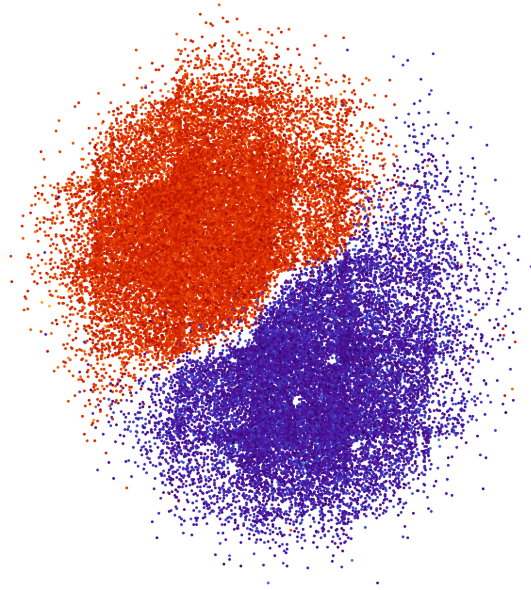


FIG. 1: A visualization of a witness simplicial complex generated from the HEPMASS particle physics data set [26] shows that this data should be easily separable by a simple non-linear manifold. A DNN will project the high-dimensional data into a lower dimensional representation with a simple separation, much like this energy-minimizing visualization does.

simple, exhibiting an easily identifiable non-linear boundary between the classes of data. By constructing a topological cover for the data, we are able to classify testing instances at nearly the level of accuracy of a DNN (88% vs. 89% and identical 96% respectively). We relate these results on large data sets to the deeper results on the smaller data

set generated by *Math Dice Jr.*, showing that the layers of the neural network have specific effects on the homology type of the data. This suggests that DNN classifiers work by attempting to simplify the topological structure of the data, which in our analysis implies easy (linear) separability. Our work hinges on a simplicial representation of the underlying data set, which can then be analyzed with tools from computational topology. The analysis in this paper focuses on binary classification [27] though the method we propose is valid for an arbitrary number of classes. We do not consider more general approximation problems [28] that can be solved with DNN's. Extending results from this work to more general approximation problems is left for future work. This work is part of a larger effort by mathematicians to understand neural networks using topological methods [29, 30]. In particular, this work is complementary to the work by Naitzat, Zhitnikov and Lim [31] who study the impact of neural network layers on the topological structure of data in classification problems. Their approach is to use persistent homology, whereas we draw inspiration from computational topology but define a specific topological structure that respects class information. Results in this paper are also related to work on the performance of deep learning as interpreted using differential topology and manifold learning. This is studied extensively by Buchanan, Gilboa and Wright [32] and Cohen et al. [33].

The remainder of this paper is organized as follows: In Section II we discuss the computational topology algorithms used throughout this paper. We study the problem of learning in Math Dice Jr. and show that training failures are correlated with the topological complexity of the underlying data set in Section III. In Section IV, we apply this analysis to two physical data sets and show that deep learning is explained by topological simplicity. Conclusions are presented in Section V. In Appendix A and Appendix B we show how to use geometric information to construct neural networks that learn Math Dice Jr.

II. VARIABLE SCALE TOPOLOGICAL DATA ANALYSIS

Most topological data analysis [34] approaches the problem of simplicial (or cubical) complex reconstruction using persistence. If $\mathcal{X} = \{\mathbf{x}_1, \dots, \mathbf{x}_N\} \subset \mathbb{R}^n$ is a set of data points, then a “pseudo-time”-varying simplicial complex \mathcal{S} is constructed from these points. The result is a filtration of complexes representing topological features at different levels of resolution. A popular approach to this is the Vietoris-Rips complex construction method, but our approach is based on the Čech complex in which each point is replaced by a ball $B_i = B_\epsilon(\mathbf{x}_i)$ and the face (i_1, \dots, i_m) is present in \mathcal{S} if and only if $B_{i_1} \cap \dots \cap B_{i_m} \neq \emptyset$. Homological analysis on \mathcal{S} can help to understand the topology of the manifold on which the data lie at the level of resolution ϵ . When ϵ is varied, the now classic persistent homology barcode [34–37] can be constructed.

In analyzing binary classification data, we are interested in features coming from the relative differences between two classes. The object is to determine whether interesting topological features emerge in the data as a result of the removal of data from a specific class. Let $\mathcal{C}_0, \mathcal{C}_1 \subset \mathcal{X}$ be two classes of data, so that $\mathcal{X} = \mathcal{C}_0 \sqcup \mathcal{C}_1$. Suppose \mathcal{X} resides on a compact Riemannian sub-manifold \mathcal{M} embedded in \mathbb{R}^n . For simplicity, we can think of \mathcal{M} as a bounding box around \mathcal{X} . The sub-manifolds \mathcal{M}_0 and \mathcal{M}_1 are compact sub-manifolds of \mathcal{M} on which \mathcal{C}_0 and \mathcal{C}_1 reside, so that if \mathcal{M}_1 and \mathcal{M}_0 intersect, they do so only at their boundaries. We assume there is an appropriately defined metric on \mathcal{M} with respect to which we will define all volumes and distances.

Let $\Omega(\mathbf{x}, \mathbf{r}) \subset \mathbb{R}^n$ be a compact set in \mathbb{R}^n that contains \mathbf{x} and whose volume is dependent on \mathbf{r} . An open ball $B_r(\mathbf{x})$ is one such example, but this formulation can be made more general so that $\Omega(\mathbf{x}, \mathbf{r})$ might be a hyper-ellipsoid, a hyper-prism etc. Without loss of generality, to find a covering of \mathcal{C}_1 that respects \mathcal{C}_0 and so that any topological features derived from the covering will be at the resolution of \mathcal{C}_0 , we solve the following independent optimization problem for each $\mathbf{x} \in \mathcal{C}_1$,

$$\begin{cases} \max_{\mathbf{r}} \text{vol}[\Omega(\mathbf{x}, \mathbf{r})] \\ \text{s.t. } \mathbf{y} \notin \Omega(\mathbf{x}_i, \mathbf{r}_i) \quad \forall \mathbf{y} \in \mathcal{C}_0 \end{cases} \quad (1)$$

When $\Omega(\mathbf{x}, \mathbf{r}) \equiv B_r(\mathbf{x})$, each problem is solvable in $O(|\mathcal{C}_0|)$. Computational examples in this paper use this simpler formulation, though more complex geometry can be used at the cost of running time.

Suppose $I_1 = \{1, \dots, |\mathcal{C}_1|\}$. Define the directed graph $\vec{G}_1 = (I_1, E_1)$

$$(i, j) \in E_1 \iff \mathbf{x}_j \in \Omega(\mathbf{x}_i, \mathbf{r}_i^*),$$

where \mathbf{r}_i^* and \mathbf{r}_j^* are the solutions to Eq. (1) for $\mathbf{x}_i, \mathbf{x}_j \in \mathcal{C}_1$. We can identify a set of witness points [38] from \vec{G}_1 by identifying a minimal dominating set $I_1^* \subset I_1$ where for each element $i \in I_1$ either $i \in I_1^*$ or there is a $j \in I_1^*$ so that $(j, i) \in E$. That is, each point \mathbf{x} in \mathcal{C}_1 is covered by some $\Omega(\mathbf{y}_i, \mathbf{r}_i)$ with $\mathbf{y}_i \in \mathcal{C}_1$. The problem of finding a minimal dominating set is known to be NP-hard [39], but can be approximated in polynomial time [40].

Using I_1^* define a new graph $S_1 = (I^*, E_1^*)$ with:

$$\{i, j\} \in E_1^* \iff \Omega(\mathbf{x}_i, \mathbf{r}_i^*) \cap \Omega(\mathbf{x}_j, \mathbf{r}_j^*). \quad (2)$$

The graph S_1 is the 1-skeleton of the Čech complex $\check{C}(S_1)$ defined by the sets $\Omega(\mathbf{x}, \mathbf{r})$ using only the witness points specified by the indices in I^* . We can also use the clique complex $\text{Cl}(S_1)$, where $\{i_1, \dots, i_m\} \in \text{Cl}(S_1)$ if and only if $\{i_1, \dots, i_m\}$ is a clique in the graph S_1 . This is often more convenient. Because \mathbf{r}_i^* is unique to each witness point \mathbf{x}_i for $i \in I^*$, this is a simplicial complex that preserves features at the scale of \mathcal{C}_0 (as a result of Eq. (1)) and where each covering element may have a different diameter. Put more concretely, when $\Omega(\mathbf{x}, \mathbf{r}_i) \equiv B_{r_i}(\mathbf{x})$, then each ball has a radius specific to its center. Also, the topological features caused by removing (e.g.) \mathcal{M}_0 from \mathcal{M} are preserved by the nerve lemma [37]. That is, we are asserting that the covering generated by $\Omega(\mathbf{x}_i, \mathbf{r}_i)$ with $i \in I^*$ is a good covering [41]. Naturally, we can perform the same construction for \mathcal{C}_0 to construct a simplicial complex representing \mathcal{M}_0 .

III. TOPOLOGICAL FEATURES OF EXAMPLE MANIFOLDS AND RESULTANT LEARNING

The game *Math Dice Jr.* is a fundamentally simple game. Three ordinary dice and two six sided dice containing only the numbers 1, 2 and 3 are rolled along with a dodecahedron. The objective is to use only addition and subtraction on the values shown on the six-sided die to arrive at the value on the dodecahedral die. For arbitrary numbers of dice, this problem can be shown to be equivalent to the NP-hard subset sum problem. In the experiments below, we consider Math Dice with 2 - 5 six-sided dice (or 3 - 6 dice overall). In all cases except the 6 dice case, we assume the 6-sided dice are ordinary (having numbers 1 - 6).

With n dice, each dice roll can be represented as a point $\mathbf{x} \in \mathbb{R}^n$. For our analysis, we define $\mathbf{x} \in \mathcal{C}_1$ if and only if all $n - 1$ six-sided dice can be used to recover the value on the n^{th} die. Determining the class of \mathbf{x} can be accomplished by solving a simple integer optimization problem (see Appendix A).

Using variable scale topological data analysis, we can construct simplicial complexes for manifolds on which the two classes of data lie. In the case when $n = 3$, we can visualize the resulting manifolds (see Fig. 2). Fig. 2 (left) shows that when $n = 3$, the submanifold \mathcal{C}_1 has a depression in which elements of \mathcal{C}_0 lie. This causes a void to emerge in the homology of $\text{Cl}(S_0)$. Likewise, the balls defining the open covering of \mathcal{M}_0 protrude through \mathcal{M}_1 as shown in Fig. 2 (right) creating holes. This leads to the Betti sequence shown in Row 1 of Table I. Here, we interpret β_i for

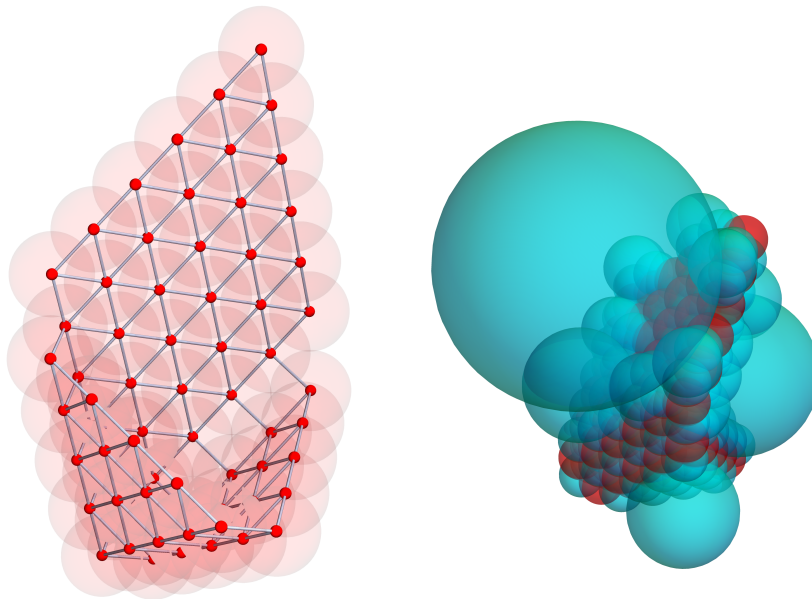


FIG. 2: (left) The 1-skeleton S_1 and covering for the manifold \mathcal{M}_1 on which dice rolls in Math Dice Jr. with 3 dice can yield the value on the dodecahedral dice. (right) The open cover of both \mathcal{M}_0 and \mathcal{M}_1 showing the two manifolds wrap around and intersect each other.

$i \geq 1$ is the number of i -dimensional holes (voids) in the simplicial complex. The number of connected components is β_0 . We compute homology for $\text{Cl}(S_1)$ for $n = 3, \dots, 6$. Betti numbers are shown in subsequent rows of Table I.

# Dice	Betti Numbers					
	β_0	β_1	β_2	β_3	β_4	β_5
3	1	12	0	0	0	0
4	1	0	357	69	0	0
5	1	0	725	4,522	12	0
6	1	0	411	72,093	250	75

TABLE I: The Betti numbers counting the numbers of components, holes and voids in the manifold \mathcal{M}_1 as estimated by the homology of $\text{Cl}(S_1)$ shows more complex structure as n increases.

Define the total number of topological features as:

$$T = \sum_{i=0}^{\infty} \beta_i.$$

As the number of dice increases, the data suggest that the total number of topological features increases exponentially (see Fig. 3). We conjecture that as the number of dice increases, the structure of the boundary between \mathcal{M}_0 and \mathcal{M}_1

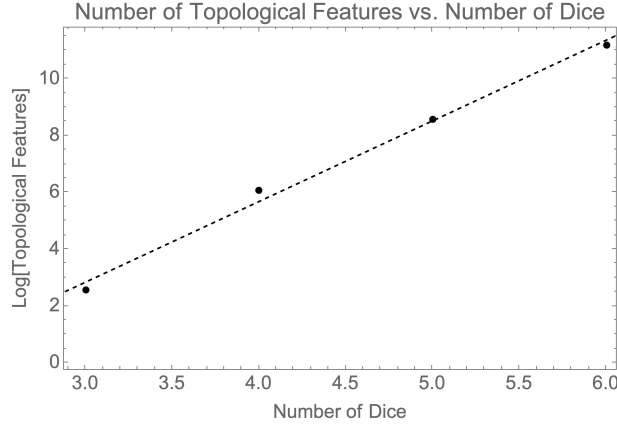


FIG. 3: The number of topological features in \mathcal{M}_1 increases exponentially as a function of the number of dice in Math Dice Jr. suggesting a complex boundary is forming between \mathcal{M}_0 and \mathcal{M}_1 .

becomes more complex, as evidenced by the exponentially increasing number of topological features in \mathcal{M}_1 as measured by the homology of $\text{Cl}(S_1)$. We illustrate the complexity of the boundary for the five dice case by constructing a joint 1-skeleton from S_1 and S_0 by creating edges between the vertices of these skeletons using Eq. (2). The resulting simplicial complex is then visualized with vertices of S_1 and S_2 shown in different colors. The image (Fig. 4), in which edges are suppressed for clarity, shows the two classes of data are thoroughly mixed as compared to Fig. 1, which is easily separable.

An increasingly complex boundary suggests that a more complex (i.e. deeper and/or wider) neural network structure is required to learn such a boundary in order to classify a sample. Table II shows evidence to support this hypothesis. In this experiment, we used a standard feedforward neural network with a ramp (ReLU) activation function between the layers and a softmax (Boltzmann distribution) as the final output layer. By way of example, the neural network structure (8, 4, 2) has a linear layer of dimension 8 with ramp activation followed by a linear layer of dimension 4 followed by a ramp followed by a linear layer of dimension 2 followed by the two class softmax classifier. All neural networks were implemented in Mathematica 13 using the built-in neural network tools. Column 3 records the mean total accuracy of the classification, and Column 4 records the minimum and maximum accuracies over a sample size of 20 random train/test splits. Notice in this experiment, the neural network complexity (as measured in number of edges) grows super-exponentially (as compared to the exponential growth in topological features). The most complex DNN used for the 6 dice case has over 10^9 connections. However, this network is not capable of separating \mathcal{C}_0 from \mathcal{C}_1 . In Appendix B we manually construct a DNN capable of properly classifying this data set and use the resulting architecture to illustrate additional challenges in learning when data sets are topologically complex.

To further understand why a large DNN fails on Math Dice Jr. with 6 dice, we analyze the behavior of DNN's that can learn Math Dice Jr. with 5 dice to determine how each layer in the network changed the topological structure of the data. Formally, we think of layer i as a function $f_i : \mathbb{R}^{n_{i-1}} \rightarrow \mathbb{R}^{n_i}$. If we exclude the final classification step,

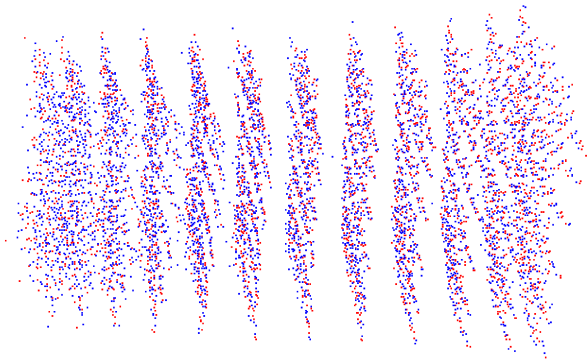


FIG. 4: Projection of witness vertices of \mathcal{S}_1 and \mathcal{S}_2 for five dice included into \mathbb{R}^5 . Edges are suppressed to improve interpretability.

Dice	DNN Struct.	Mean Acc.	(Min, Max)
3	(8,4,2)	0.93	(0.78, 1.)
3	(16,4,2)	0.98	(0.85, 1.)
4	(16,4,2)	0.88	(0.79, 0.97)
4	(32,4,2)	0.94	(0.82, 0.99)
5	(128,16,2)	0.91	(0.81, 0.95)
5	(256,16,2)	0.94	(0.88, 0.98)
6	(1024,256,64,16,2)	0.56	(0.52, 0.63)
6	(2048,256,64,16,2)	0.54	(0.49, 0.56)

TABLE II: Even when the complexity of the neural network structure required grows super-exponentially, a 5-layer DNN with over 10^9 connections cannot learn the boundary structure between \mathcal{C}_1 and \mathcal{C}_0 in 6 dice Math Dice Jr.

the neural network is simply a function $f : \mathbb{R}^N \rightarrow \mathbb{R}^2$ such that $f = f_L \circ \dots \circ f_1$. If f is a homeomorphism, then f cannot change the homology of the underlying manifolds. However, since we are interested in homological features up to the level of resolution of (e.g.) Class 0 within Class 1, we expect to see a topological simplification taking place at each level. The data in Table III support this hypothesis. The data were generated using the complete 5 dice Math

	Betti Numbers					
Layer	β_0	β_1	β_2	β_3	β_4	β_5
0 (Input)	1	0	725	4,522	12	0
1	1	0	0	570.	303.	0.
2	20.2	12.3	0.9	0.1	0	0
3	9.45	2.4	0	0	0	0

TABLE III: The topological complexity of the boundary between \mathcal{M}_0 and \mathcal{M}_1 is further simplified and refined at each layer of a neural network that successfully classifies Math Dice Jr.

Dice Jr. data set and training a neural network with structure (256, 16, 2). The classifier layer was then removed and the original 5 dice data set was transformed (by $f_{L-1} \circ \dots \circ f_1$). Homological information on the clique complex for this lower dimensional data set was then computed. This process was repeated for hidden layers two and one. We repeated this in 20 replications (to average out effects from stochastic gradient descent). Table III shows mean Betti numbers (indicating topological structure) for these 20 runs. As shown in Fig. 5, the number of topological features in the data decreases exponentially in each layer. Note this is similar to the results identified by Naitzat, Zhitnikov and Lim [31] in their independent study. This supports the hypothesis that each layer is simplifying the boundary structure between the two classes of data. We compare this to the topological complexity of the data output by the last layer of a neural network with structure (2048, 256, 64, 16, 2) acting on 6 dice Math Dice Jr. data, which we know from Table II cannot successfully identify the boundary structure between \mathcal{M}_0 and \mathcal{M}_1 . In an example run, the data produced by the final layer is disconnected into several thousand components, showing that the neural network has mapped the two classes onto each other, explaining the confusion and low accuracy in the last row of Table II. By the universal approximation theorem [42, 43] there is a neural network that can approximate \mathcal{M}_0 and \mathcal{M}_1 in the 6 dice Math Dice Jr. case, however finding the simplest such neural network structure is clearly non-trivial, consistent

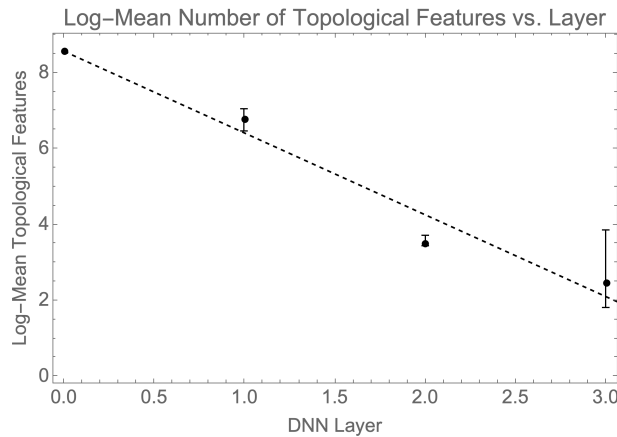


FIG. 5: The topological complexity of the transformed data decreases exponentially with each layer, ultimately making classification trivial.

with the no free lunch theorem [21, 22]. As noted, in Appendix B we use geometric information to construct a neural network architecture that can be successfully trained for this problem. Determining the exact cause of the failure (e.g., vanishing gradient problems or modeling settling) and how this relates to the topological complexity is left as a future area of research.

IV. APPLICATION TO PHYSICAL DATA SETS

We describe two experiments on physical data known to be amenable to classification by deep learning methods. We show that both data sets exhibit simple topological structure, explaining the ability of deep learning methods to classify these data structures.

A. HEPMASS Data

To test the scalability of the cover generation approach, we used the open source HEPMASS dataset [26], which is composed of 10.5M Monte Carlo simulations of high-energy particle collisions. The data is divided into 7M simulations where the signal particle has mass equal to a nominal 1000 with the remaining examples having variable mass. We used the 7M samples with fixed mass 1000. The data resides in 27 dimensional Euclidean space.

Testing suggests the data is amenable to classification by DNN [44]. To explain this, we constructed the two simplicial complexes S_1 and S_2 using open balls for the topological covering. Because the data set is large (by the standards of most topological data analysis algorithms), we cannot compute a complete set of topological features. Graph-theoretic analysis suggests that the two manifolds \mathcal{M}_1 and \mathcal{M}_0 are largely connected. The manifold \mathcal{M}_1 consists of a giant component with a second small disconnected component, which maps to an isolated vertex in the simplicial complex S_1 . The manifold \mathcal{M}_0 is path connected. Information on the topological structure is shown in Table IV. Despite the fact that we cannot extract more specific topological information using commodity hardware,

Class	Sample Size	Complex Size	β_0
Class 1	3,500,879	2,949,847	2 (1 dimension 0)
Class 0	3,499,129	2,040,509	1

TABLE IV: High level topological features of the HEPMASS data set. Here, 0 dimensional simplexes are isolated vertices in S_1 or S_0 .

it is possible to measure the goodness of the cover (and thus its ability to render topological information) by using a train/test split, which can also be compared to the outputs of a DNN. To speed up computation, 150,000 balls from the topological coverings defining S_1 and S_2 were chosen at random. This effectively produced a witness complex [38] containing 300,000 points. We refer to this as the witness cover. The resulting witness complex skeletons are

visualized in Fig. 1, which shows a high degree of separability between the two classes, implying that these classes should be easily separated from the topological perspective.

We used 20 random samples of the HEPMASS testing data set, each of size 20,000. A sample was declared to be in Class 1 if it was contained in a witness cover element of Class 1 and not of Class 0. To deal with ambiguities, samples that appeared in both covers (confused samples) were assigned to the class of the cover they were closer to in the Euclidean metric. Samples that were outside both covers were likewise assigned to the class of the cover they were closer to in the Euclidean metric. Results of this experiment are shown in Table V. The data suggest that the

Measures	Mean	(Min,Max)
Total Accuracy	0.881	(0.879, 0.885)
True Positive	0.897	(0.893, 0.901)
False Positive	0.134	(0.13, 0.139)
F1 Score	0.883	(0.861, 0.887)
Out of Cover Proportion	0.547	(0.54, 0.553)
Confused Cover Proportion	0.00326	(0.00275, 0.00383)

TABLE V: Results show mean total accuracy of 88% with similar true positive and F1 scores. Interestingly, 55% of the test data (on average) was outside the cover, meaning substantial generalization was required. Only 0.3% of the test data fell close enough to the boundary to lie in both covers.

cover accurately respects the topological structure of \mathcal{M}_1 and \mathcal{M}_0 including the boundary, with only 0.33% of test samples confused between the two covers. However, testing samples frequently fall outside the specific boundaries of the cover, which would require generalization from a neural network classifier. This may be a result of our use of a witness cover. Based on these results, we expect to see high-quality separation from a DNN. To test this hypothesis, we used a DNN with architecture (128, 64, 32, 2) ending in a softmax classifier and tested on 20 replications of 20,000 test points chosen at random. Results are shown in Table VI and are consistent with [44]. Unsurprisingly, the neural

Measures	Mean	(Min, Max)
Total Accuracy	0.89	(0.888, 0.8886)
True Positive	0.89	(0.878, 0.891)
False Positive	0.12	(0.116, 0.129)
F1 Score	0.88	(0.88, 0.887)

TABLE VI: Results show mean total accuracy of 88% with similar true positive and F1 scores. The false positive rate is slightly lower than the false positive rate of the topology-based classifier.

network outperforms the naïve topology-based classification method, but only by 1% on average. We attribute this to (i) improved ability to model the separating boundary and (ii) better generalization. However, the topological simplicity of the underlying data clearly explains a substantial portion of the DNN’s success.

B. Undersea Acoustic Data

We performed a similar analysis on open source data provided by the Scripps Institute [45] consisting of Fourier transforms of undersea acoustic data. There were $\approx 1.5M$ samples from *Lagenorhynchus obliquidens*. Class 1 was composed of Type A clicks and Class 0 was composed of Type B clicks. This data set is fully described and analyzed using a Deep Neural network in [45], where it is shown empirically the data are amenable to classification by DNN. Topological analysis shows that the data are composed of path connected manifolds residing in 181 dimensional Euclidean space. There are no disconnected elements, though again the data are too large to allow for complete topological investigation. A summary of the gross topological properties of S_1 and S_2 is given in Table VII. As before,

Class	Sample Size	Complex Size	β_0
Class 1	798,116	320,777	1
Class 0	679,894	374,763	1

TABLE VII: High level topological features of the Scripps data set. Both S_1 and S_0 have one component ($\beta_0 = 1$) implying the underling manifolds on which Type A and Type B clicks reside are path connected.

we created a visualization of the joint S_1 and S_0 simplexes, shown in Fig. 6. Interestingly, this visualization suggests

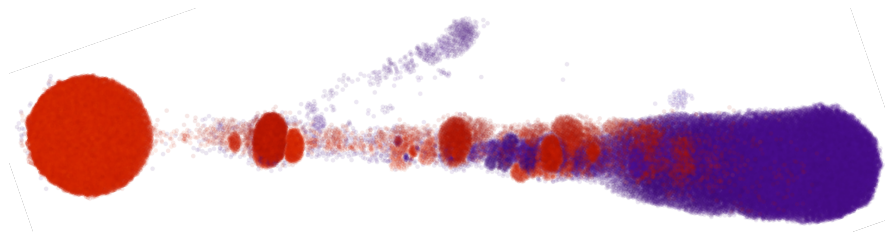


FIG. 6: Visualization of the witness simplicial complex of the two click classes of *Lagenorhynchus obliquidens*.

the data are more complex than the corresponding HEPMASS data. Further topological analysis is required to prove this is true.

To test the goodness of a covering generated by a subset of this data, we removed 20,000 samples from each class and rebuilt a topological covering with the remaining data. We used the same method for classifying test data as for HEPMASS. The data suggest that 96% accuracy can be achieved using the topological classifier, with only 4.5% of test samples confused between the two classes. In this test, 19% of the test data was outside the cover. Complete results are shown in Table VIII. A DNN with architecture (1024, 128, 64, 32, 2) ending in a softmax classifier was also

Measures	Value
Total Accuracy	0.96
True Positive	0.96
False Positive	0.042
F1 Score	0.96
Out of Cover Proportion	0.19
Confused Cover Proportion	0.045

TABLE VIII: Results show a total accuracy of 96% with 96% true positive and F1 score 0.96. Interestingly 19% of the test data (on average) was outside the cover, meaning some generalization was required. Only 4.5% of the test data fell close enough to the boundary to lie in both covers.

trained on the data. The total accuracy using this DNN was also 96%, with a slightly lower false positive rate than the topological approach, but not considerably so. This suggests the DNN may be slightly better at generalizing the complex boundary structure than the open sets forming the covering of the topology. Full test results are in Table IX. In this case, it is surprising that the DNN only outperforms the naïve topology-based classification method

Measures	Value
Total Accuracy	0.96
True Positive	0.96
False Positive	0.036
F1 Score	0.96

TABLE IX: Results show a total accuracy of 96% with similar true positive and F1 scores. The false positive rate is lower than the topology-based classifier, suggesting better generalization.

in false positive rate. However, we can again assert the topological simplicity of the underlying data clearly explains a substantial portion of the DNN's success, especially when contrasted with the failure of learning in 6 dice Math Dice Jr., where the topological structure of the manifolds \mathcal{M}_0 and \mathcal{M}_1 are more complex even though the data sets are much smaller.

V. CONCLUSIONS AND FUTURE DIRECTIONS

In this paper, we have shown that the ability of an *ad hoc* DNN to learn to classify data successfully is highly dependent on the topological structure of the underlying Riemannian manifolds on which the data lie. Using an illustrative example taken from a simple children's game, we constructed a data set whose topological complexity grew exponentially. We showed that DNN's that successfully learned how to separate high-scoring states from lower scoring states exponentially decreased the topological complexity of the data in each subsequent layer of the network.

In cases where a DNN was unable to learn to separate the classes, we showed that the network failed to reduce the topological complexity of the data. Interestingly, learning failure occurred when the topological complexity of the data was highest. We then applied these techniques to two large physical data sets (one from particle physics and the other from ocean acoustics) known to be amenable to classification by DNN. We showed their topological complexity was comparatively low and that the majority of the DNN's ability to classify these data sets was explained by information available in a topological covering. Additional work (in progress) should show that their topological complexity as measured by the quantity T is also low, with an estimate of fewer than 10 topological voids (all dimensions) in the acoustic data set and no voids in the HEPMASS data set. We leave complete details of this analysis to a future paper. This study suggests that further investigation into large-scale topological data analysis, including the automated extraction of information on manifold boundaries, may help explain how DNN's function as well as the limitations these methods have.

Appendix A: Integer Programming Solution to Math Dice Jr.

All Math Dice Jr. games with n dice can be solved using a simple integer programming problem:

$$\left\{ \begin{array}{l} \max \sum_{i=1}^{n-1} x_i + y_i \\ s.t. \quad x_i + y_i \leq 1 \quad \forall i \\ \sum_{i=1}^{n-1} d_i(x_i - y_i) = d_n \\ 0 \leq x_i, y_i \leq 1 \quad \forall i \\ x_i, y_i \in \mathbb{Z} \quad \forall i. \end{array} \right.$$

Here, a die value d_i (for die i) is added if $x_i = 1$ and subtracted if $y_i = 1$. We are maximizing the number of dice used, which is given by $(x_1 + y_1) + \dots + (x_{n-1} + y_{n-1})$ because the first constraint $x_i + y_i \leq 1$ along with the third and fourth constraints ensure that exactly one of x_i or y_i is 1 but both may be zero (if a die is not used). The second constraint ensures that the resulting sum equals the value shown on the n^{th} die (the dodecahedron). Using this formulation, we solved the 23,328 distinct Math Dice Jr. rolls (with 6 dice) in 19.05 s.

Appendix B: Customized DNN for Classifying Math Dice Jr.

As noted, the failure of a single feedforward neural network architecture does not necessarily imply that a problem cannot be solved easily with a neural network. The topological covering identified by the method discussed in Section II can be transformed into a feed-forward neural network by creating a polygonal approximation of the covering sets and using a neural encoding of the boolean logic testing where a vector \mathbf{x} lies with respect to this cover. However, this may lead to unacceptably large (though not fully connected) networks. Instead, we demonstrate a simple architecture with hand-coded weights for this problem that readily solves 6 dice Math Dice Jr. We then show that learning still fails without these hand-coded weights.

Let $\mathcal{W} = \{-1, 1\}^5 \subset \mathbb{R}^5$. Let $\mathcal{R} \subset \mathbb{R}^6$ be the set of possible rolls in 6 dice Math Dice Jr. For $\mathbf{w} \in \mathcal{W}$ and $\mathbf{x} \in \mathcal{R}$, let:

$$\varphi(\mathbf{x}; \mathbf{w}) = \sum_{i=1}^5 w_i x_i - x_6.$$

Let:

$$\tilde{\delta}(x) = \begin{cases} 1 & x = 0 \\ 0 & \text{otherwise.} \end{cases}$$

Choose an order so that $\mathcal{W} = \{\mathbf{w}_1, \dots, \mathbf{w}_{32}\}$. Then the function, $\mathbf{F} : \mathbb{R}^6 \rightarrow \mathbb{R}^{32}$ defined by:

$$\mathbf{F}_i(\mathbf{x}) = \tilde{\delta}[\varphi(\mathbf{x}; \mathbf{w}_i)],$$

maps each roll to a vertex on the unit hypercube \mathbb{R}^{32} . For a roll \mathbf{x} , all five hexahedral die can be used to obtain the number on the dodecahedral die if and only if $\mathbf{F}(\mathbf{x}) \neq \mathbf{0}$ (the vector of all zeros). Any linear separator that separates the vertex $\mathbf{0}$ from the other vertices of the unit hypercube in \mathbb{R}^{32} will correctly classify this point. This is the explicit mapping in Cover's theorem [46].

For simplicity, let $\sigma : \{0, 1\}^{32} \rightarrow \{0, 1\}$ so that:

$$\mu(\mathbf{y}) = \max_i y_i.$$

Then the function that classifies any roll $\mathbf{x} \in \mathbb{R}$ is given by:

$$C(\mathbf{x}) = \mu[\mathbf{F}(\mathbf{x})] = \mu\{\tilde{\delta}[\varphi(\mathbf{x}; \mathbf{w}_i)]\}.$$

This can be encoded in the feedforward neural network architecture shown in Fig. 7. It is straightforward to generalize

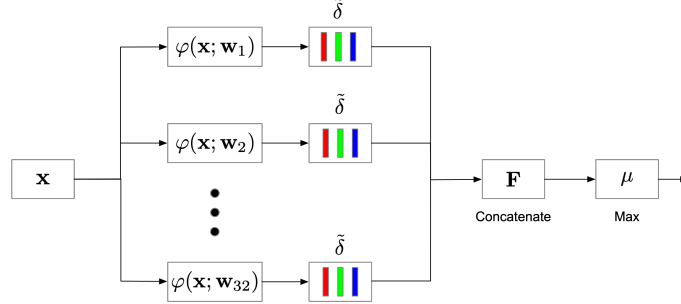


FIG. 7: A custom feed forward neural network architecture that will correctly classify all rolls in 6 dice Math Dice Jr. This architecture can be easily generalized to arbitrary Math Dice Jr. games.

this architecture for an arbitrary Math Dice Jr. game by scaling \mathcal{W} .

We can analyze the topological structure of the data produced by the layers of this neural network. We note that using the mapping $\mathbf{F}(\mathbf{x})$ to transform the data into thirty-two dimensional points creates a 1-skeleton that is the complete graph on the 49 open spheres that can be used to cover $\mathbf{F}(\mathcal{R})$. Thus, all voids are closed by this mapping and the data fully separates into two manifolds that are contractible to a single point. (Obviously, class zero contracts exactly to a point.)

For 6 dice Math Dice Jr., the function $\hat{\delta}$ can be approximated using a simple (64, 16, 4, 1) feedforward neural network, with the final layer being a logistic sigmoid rather than a softmax classifier. We used three separate experimental protocols on this architecture.

1. (Weights with Separate Training) All weights from \mathcal{W} were pre-set, and we separately trained the neural network implemented $\hat{\delta}$ using values from $\varphi(\mathbf{x}; \mathbf{w}_i)$ for a random train/test sample from \mathcal{R} . We then glued the network architecture shown in Fig. 7 together from the pre-trained or specified components.
2. (Architecture Only) No weights from \mathcal{W} were used and $\hat{\delta}$ was not pre-trained. Only the architecture shown in Fig. 7 was used and was trained on a random train/test sample.
3. (Weights with Joint Training) Weights from \mathcal{W} were pre-set and the architecture shown in Fig. 7 was used but $\hat{\delta}$ was not separately trained. The complete network was trained on a random train/test split.

Results using an 85%/15% train/test split with 20 replications are shown in Table X. When the weights in \mathcal{W} are

Experiment	Mean Acc.	(Min, Max)
Weights/Separate Training	0.907	(0.524,1)
Architecture Only	0.553	(0.535,0.624)
Weights/Joint Training	0.832	(0.453,1)

TABLE X: Experimental results showing mean accuracy when a custom neural network architecture is used with and without pre-set weights that ensure success.

manually specified the performance increase is, substantial with most testing results yielding 100% accuracy, which

is achievable if $\hat{\delta}$ is correctly approximated. When no weights are pre-specified, the results are similar to the ones presented in naïve feed forward networks in Section III.

-
- [1] H.-C. Ruiz Euler, M. N. Boon, J. T. Wildeboer, B. van de Ven, T. Chen, H. Broersma, P. A. Bobbert, and W. G. van der Wiel, *Nature nanotechnology* **15**, 992 (2020).
 - [2] J. Collins, K. Howe, and B. Nachman, *Physical review letters* **121**, 241803 (2018).
 - [3] G. Graziano, *Nature Reviews Chemistry* **4**, 564 (2020).
 - [4] X. Liu, G. Zhang, J. Li, G. Shi, M. Zhou, B. Huang, Y. Tang, X. Song, and W. Yang, *Physical review letters* **124**, 113202 (2020).
 - [5] J. R. Moreno, G. Carleo, and A. Georges, *Physical Review Letters* **125**, 076402 (2020).
 - [6] N. Sun, J. Yi, P. Zhang, H. Shen, and H. Zhai, *Physical Review B* **98**, 085402 (2018).
 - [7] Z. T. Wang, Y. Ashida, and M. Ueda, *Physical Review Letters* **125**, 100401 (2020).
 - [8] J. Hermann, Z. Schätzle, and F. Noé, *Nature Chemistry* **12**, 891 (2020).
 - [9] R. Iten, T. Metger, H. Wilming, L. Del Rio, and R. Renner, *Physical review letters* **124**, 010508 (2020).
 - [10] K. Atz, F. Grisoni, and G. Schneider, *Nature Machine Intelligence* , 1 (2021).
 - [11] Z. Liu and M. Tegmark, *Physical Review Letters* **126**, 180604 (2021).
 - [12] A. E. Allen and A. Tkatchenko, *Science Advances* **8**, eabm7185 (2022).
 - [13] J. Carrasquilla and R. G. Melko, *Nature Physics* **13**, 431 (2017).
 - [14] C. L. Ritt, M. Liu, T. A. Pham, R. Epsztein, H. J. Kulik, and M. Elimelech, *Science advances* **8**, eabl5771 (2022).
 - [15] A. Seif, M. Hafezi, and C. Jarzynski, *Nature Physics* **17**, 105 (2021).
 - [16] C. B. Wahl, M. Aykol, J. H. Swisher, J. H. Montoya, S. K. Suram, and C. A. Mirkin, *Science advances* **7**, eabj5505 (2021).
 - [17] M. Schmitt and M. Heyl, *Physical Review Letters* **125**, 100503 (2020).
 - [18] M. Dax, S. R. Green, J. Gair, J. H. Macke, A. Buonanno, and B. Schölkopf, *Physical review letters* **127**, 241103 (2021).
 - [19] G. Kántor, C. Papageorgakis, and V. Niarchos, *Physical Review Letters* **128**, 041601 (2022).
 - [20] K. Kottmann, P. Huembeli, M. Lewenstein, and A. Acín, *Physical Review Letters* **125**, 170603 (2020).
 - [21] D. H. Wolpert, *Neural computation* **8**, 1341 (1996).
 - [22] D. H. Wolpert and W. G. Macready, *IEEE transactions on evolutionary computation* **1**, 67 (1997).
 - [23] R. Brierley, *Nature Physics* **18**, 373 (2022).
 - [24] K. Sharma, M. Cerezo, Z. Holmes, L. Cincio, A. Sornborger, and P. J. Coles, *Physical Review Letters* **128**, 070501 (2022).
 - [25] N. Jones, *Nature* (2009), 10.1038/news.2009.914.
 - [26] P. Baldi, K. Cranmer, T. Faucett, P. Sadowski, and D. Whiteson, *arXiv preprint arXiv:1601.07913* (2016).
 - [27] R. Kumari and S. K. Srivastava, *International Journal of Computer Applications* **160** (2017).
 - [28] D. Elbrächter, D. Perekrestenko, P. Grohs, and H. Bölskei, *IEEE Transactions on Information Theory* **67**, 2581 (2021).
 - [29] B. Hanin and M. Sellke, “Approximating continuous functions by relu nets of minimal width,” (2017), *arXiv:1710.11278 [stat.ML]*.
 - [30] J. E. Grigsby and K. Lindsey, *SIAM Journal on Applied Algebra and Geometry* **6**, 216 (2022).
 - [31] G. Naitzat, A. Zhitnikov, and L.-H. Lim, *J. Mach. Learn. Res.* **21**, 1 (2020).
 - [32] S. Buchanan, D. Gilboa, and J. Wright, *arXiv preprint arXiv:2008.11245* (2020).
 - [33] U. Cohen, S. Chung, D. D. Lee, and H. Sompolinsky, *Nature communications* **11**, 1 (2020).
 - [34] G. Carlsson, *Bulletin of the American Mathematical Society* **46**, 255 (2009).
 - [35] R. Ghrist, *Bulletin of the American Mathematical Society* **45**, 61 (2007).
 - [36] J. R. Munkres, *Elements of algebraic topology* (CRC press, 2018).
 - [37] H. Edelsbrunner and J. Harer, *Computational Topology: An Introduction* (2010).
 - [38] V. De Silva and G. E. Carlsson, *SPBG* **4**, 157 (2004).
 - [39] S. T. Hedetniemi and R. C. Laskar, in *Annals of Discrete Mathematics*, Vol. 48 (Elsevier, 1991) pp. 257–277.
 - [40] A. K. Parekh, *Information processing letters* **39**, 237 (1991).
 - [41] P. Petersen, *Riemannian geometry*, Vol. 171 (Springer, 2006).
 - [42] G. Cybenko, *Mathematics of control, signals and systems* **2**, 303 (1989).
 - [43] G. Cybenko, *Math. Control. Signals Syst.* **5**, 455 (1992).
 - [44] A. Mavuduru, “How deep learning can solve problems in high energy physics,” <https://towardsdatascience.com/how-deep-learning-can-solve-problems-in-high-energy-physics-53ed3cf5e1c5> (2021).
 - [45] K. E. Frasier, *PLoS Computational Biology* **17**, e1009613 (2021).
 - [46] T. M. Cover, *IEEE transactions on electronic computers* , 326 (1965).